Thin Solid Films 519 (2011) 8030–8036

Contents lists available at ScienceDirect

Thin Solid Films

journal homepage: www.elsevier.com/locate/tsf

On the photoluminescence of multilayer arrays of silicon rich oxide with high silicon content prepared by low pressure chemical vapor deposition

E. Quiroga-González [a], W. Bensch [b], M. Aceves-Mijares [c,*], Z. Yu [d], R. López-Estopier [e], K. Monfil-Leyva [f]

[a] Institute for Materials Science of the University of Kiel, Kaiserstr. 2. D-24143 Kiel, Germany
[b] Institute for Inorganic Chemistry of the University of Kiel, Max-Eyth-Str. 2. D-24118 Kiel, Germany
[c] National Institute for Astrophysics, Optics and Electronics, Luis Enrique Erro 1, 72840 Tonantzintla, Mexico
[d] Solar Energy Division, Tianjin Lishen Battery Joint-Stock Co Ltd. 300384 Tianjin, China
[e] Instituto Tecnológico Superior de Poza Rica, Luis D. Colosio S/N, 93230 Poza Rica, Mexico
[f] Centro de Investigación en Energía-UNAM, Privada Xochicalco S/N, 62580 Temixco, Mexico

ARTICLE INFO

Article history:
Received 19 May 2010
Received in revised form 2 June 2011
Accepted 10 June 2011
Available online 15 June 2011

Keywords:
Multilayers
Silicon rich oxide
Nanoparticles
Photoluminescence
Low-pressure chemical vapor deposition
Transmission electron microscopy

ABSTRACT

The photoluminescence emission of multilayer structures composed of layers of silicon rich oxide with high silicon content and layers of silicon rich oxide with low silicon content obtained by low pressure chemical vapor deposition is here presented. Different parameters for the preparation of the multilayers have been varied such as the Si concentration and the thicknesses of the layers. Additionally, the samples were oxidized at different temperatures. For all samples the photoluminescence seems to have the same origin: defects in the oxide matrix and defects at the interfaces between the Si nanocrystals. The structural and compositional properties of the multilayer structures are discussed.

1. Introduction

Multilayer structures (MLs) and superlattices containing Si nanocrystals (Si-NCs) have received much attention during the last years due to the many application possibilities, for example in third generation solar cells [1]. Fabricating tandems of layers based on Si and its oxides with Si being present as quantum dots, the band gap of an upper cell material can be engineered [2], where the Si-NCs exhibit a three dimensional quantum confinement effect. The size of the Si-NCs can be tuned adjusting the thickness of the layers [3].

ML structures with Si NCs have been also prepared to perform size-dependent photoluminescence (PL) studies of the Si-NCs [3]. The layers containing Si-NCs can be prepared by different methods, like implantation of Si in an amorphous matrix (principally SiO_2) [4,5], or deposition of silicon rich oxides (SRO) [6,7]. In the case of SRO, which are also called off-stoichiometric silicon oxide or silicon rich silicon oxide, the Si-NCs grow by segregation of the Si excess from the silicon oxides during thermal treatments at elevated temperatures [8]. An indicator of the Si content in such materials is the parameter Ro, which is the ratio of the partial pressure of the precursor gases (for example, N_2O/SiH_4) when it is prepared by gas phase deposition methods like CVD (Chemical Vapor Deposition). Among CVD methods, the Low Pressure Chemical Vapor Deposition (LPCVD) is a very convenient approach for the deposition of SRO films because it allows an exact variation of the Si content, and CVD is a simple and cheap preparation method.

Single layers of SRO with low Si excess usually exhibit PL, but the PL signal is caused by different effects that cannot be easily separated due to a large dispersion of the Si-NC sizes. There are some reports on the origin of the PL of Si-NCs in silicon oxides distinguishing between the PL due to quantum confinement effects and the PL caused by defects [9], and different kinds of defects responsible for the PL were also identified [10]. Nevertheless there is still some uncertainty concerning the real origin of the PL signal observed for samples prepared by different techniques, and with different post thermal treatments and particle size ranges. For example, in single films of SiO_x prepared by evaporation, the PL is dominated by defects when the annealing temperatures are below 900 °C and the PL has a component caused by quantum confinement effects when the temperatures are above 1000 °C [11]. The PL signal due to quantum confinement effects in Si-NCs has also been observed in Si-implanted SiO_2 films where the PL peak blue-shifted with oxidation time [5], with the largest particles in these films being about 5 nm. The blue-shift has also been observed for sputtered SRO films when the Si-NCs sizes vary from 2.7 to 5 nm [12,13]. SRO films prepared by LPCVD present intense PL when their Si excess (excess compared to SiO_2) is

* Corresponding author. Tel.: +52 222 2470517.
E-mail address: maceves@ieee.org (M. Aceves-Mijares).

0040-6090/$ – see front matter © 2011 Elsevier B.V. All rights reserved.
doi:10.1016/j.tsf.2011.06.020

lower than 8 at.% (Ro = 20–30), and a weak emission was found for an excess larger than 12 at.% (Ro<10) [6,14]. A very small blue-shift of the PL signal is observed going from SRO Ro = 20 to Ro = 30, i.e. for particle sizes of around 2.75 nm and no observable particles, respectively, but no such shift occurred when the Ro was reduced to 10 leading to Si-NCs sizes of around 4.2 nm [6]. These findings indicate that the PL in such types of films is dominated by defects.

An evident blue-shift in the PL could be observed in evaporated MLs containing Si-NCs when the size of the nanocrystals decreases from 3.2 nm to 2.8 nm [3], an effect that was ascribed to quantum confinement effects. For a study of the quantum confinement effects the Si content in the layers containing Si-NCs should be large in order to assure the tuning of the Si-NC sizes with the thickness of the layers.

In the present work we report a structural study of MLs prepared by LPCVD containing SRO with high silicon content (Ro ≤ 3). Selected properties of such ML structures of SRO prepared by LPCVD have been previously reported by our group [15]. The PL properties of MLs with SRO with different Si content, different Si-NC sizes, and oxidized at different temperatures are compared in the present study. Transmission Electron Microscopy (TEM), X-ray Photoelectron Spectroscopy (XPS) and ellipsometry were used to characterize the structural and compositional properties of the MLs. The properties of single layers of SRO were also analyzed in order to acquire information about the constituents of the MLs and related effects.

2. Experimental details

SRO single layers with Ro = 1 (SRO1), Ro = 3 (SRO3), Ro = 30 (SRO30) and Ro = 50 (SRO50), and ML structures composed of stacks of SRO1 (or SRO3) and SRO50 were deposited on p-type Si (100) wafers with 30–50 Ωcm resistivity by LPCVD at 725 °C. For the preparation of the materials SiH_4 and N_2O were applied as precursor gases. The experimental details about the single layers and ML structures are summarized in Table 1. The MLs composed of n + 1 layers of material 1 (SRO50) and n layers of material 2 (SRO1 or SRO3) were deposited varying manually the amount of the precursor gases during the deposition process. Afterwards the samples were annealed in N_2 at 1100 °C for 3 h to induce nucleation of the Si-NCs.

The microstructure of the MLs was studied with TEM measurements (Tecnai F30, 300 kV). A Null ellipsometer Gaertner L117, which operates with a 632.8 nm laser at a fixed 70° angle of incidence, was used to determine the refractive index of the samples. XPS analysis was carried out with an electron spectrometer (Omicron) equipped with a non-monochromated Al Ka source at 0° take off angle. For these measurements, the samples were previously sputtered in a preparation chamber (Omicron Full Lab) bombarding the samples with argon ions with a kinetic energy of 1 keV at an incident angle of 36° for 5 min. The PL emission spectra were measured with a spectrofluorometer Jobin Yvon Fluoromax-3 at room temperature; the samples were excited with energy of 280 nm (4.42 eV), and a long-pass filter of 400 nm (3.1 eV) in the detector was used.

Table 1
As deposited samples.

Sample	Number of periods	Material 1	Material 1 expected thickness [nm]	Material 2	Material 2 expected thickness [nm]	Total thickness [nm]
SRO1	Single layer	SRO1	133	–	–	133
SRO3	Single layer	SRO3	72	–	–	72
SRO30	Single layer	SRO30	400	–	–	400
SRO50	Single layer	SRO50	60.8	–	–	60.8
M1	7	SRO50	4	SRO3	4	53
M2	3	SRO50	7	SRO3	8.5	38
M3	5	SRO50	12	SRO1	22	150

The thickness of the layers is an estimated value given for the deposition rate of single layers.

3. Results and discussion

3.1. SRO single layers

The composition of SRO30 and SRO50 prepared under similar conditions as in the present case have been already reported in different articles [15,16]. For the sample SRO30 a Si excess of around 6 at.% was observed [16], which is present in the oxide matrix as amorphous Si sub-oxides but not as Si-NCs [17]. On the other hand, SRO50 is a material with composition very close to stoichiometric SiO_2 [15].

The composition of the materials with high Si contents (SRO1 and SRO3) was determined with XPS analyses on single films of these materials. The Si 2p peak exhibits the $2p_{3/2}$ and $2p_{1/2}$ spin-orbit splitting with the two levels being separated by 0.6 eV [18]. The positions of the peaks corresponding to Si^0 (elemental Si) and Si^{4+} (SiO_2) are easily distinguishable in the XPS spectra of SRO1 and SRO3 (Fig. 1a and b respectively), and the assignment of these two different Si species is straightforward using literature data [18,19]. The $2p_{3/2}$ signal of elemental Si occurs at around 99 eV with the corresponding $2p_{1/2}$ line located 0.6 eV at higher energies. The $2p_{3/2}$ signal of SiO_2 is significantly shifted to higher binding energies by about 4 eV and appearing at around 103 eV. The peaks of the Si sub-oxides are located in the region between these two Si species. Because an unambiguous individual assignment of SiO_x sub-oxides is not possible, all sub-oxides are considered as one group. The amount of sub-oxides in the samples was estimated by subtracting the area of the fitted peaks of Si^0 and Si^{4+} from the total area. The binding energies of the peaks

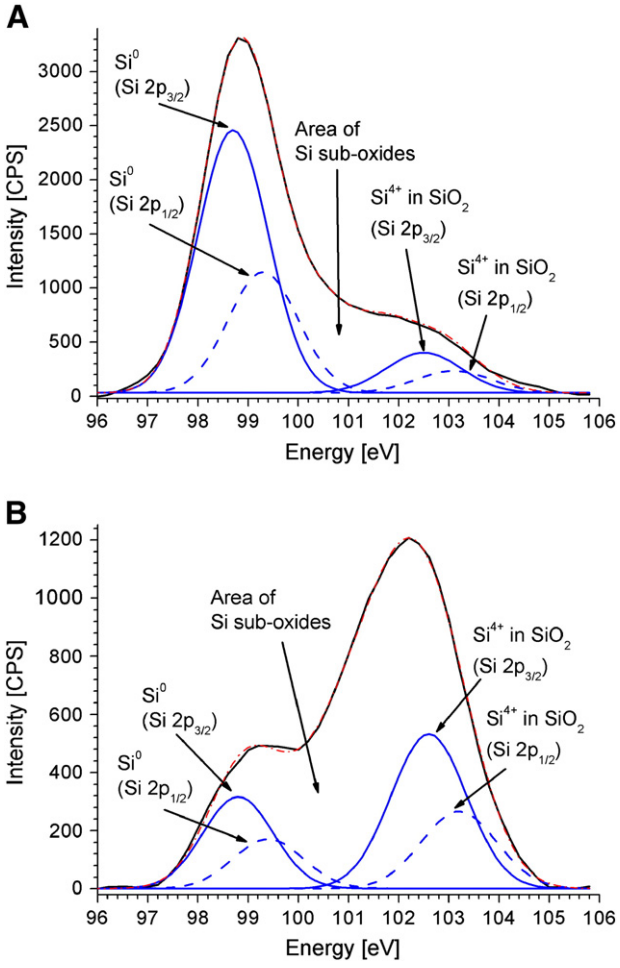

Fig. 1. XPS spectrum of a) SRO1 and b) SRO3. The peaks of the Si $2p_{1/2}$ and Si $2p_{3/2}$ of Si^0 and Si^{4+} were fitted. Sub-oxide species are found in the region between Si^0 and Si^{4+}.

related with silicon sub-oxides have been reported for Si/SiO_2 interfaces [18,20], but they cannot be distinguished unequivocally in a complex spectrum composed of different Si oxides. Hence, a quantitative analysis of such highly convoluted spectra is not straightforward and the results obtained by fitting procedures sensitively depend on the fitting parameters applied. According to the deconvolution of the XPS spectra, SRO1 is composed of 72, 12 and 16 at.% of elemental Si, SiO_2 and SiO_x ($0<x<2$), while SRO3 contains 20, 34 and 46 at.% of these materials, respectively. The amount of elemental Si in SRO1 is about 3.6 times larger than in SRO3. In a previous X-ray diffraction (XRD) study we estimated the average size of the Si-NCs in single layers of SRO1 to be about 30 nm [21]. A similar estimation of the size of the NCs in SRO3 using XRD was less straightforward because the amount of Si-NCs is very small leading to very broad Bragg reflections with low intensity. Hence, the data for the average size of the NCs in SRO3 are not very reliable.

When analyzing the PL emission of the SRO single layers, only SRO30 presented a PL signal detectable by the measurement system. This means that neither materials with high Si contents (SRO1 and SRO3) nor those with composition close to SiO_2 (SRO50) exhibit detectable PL signals. The PL spectrum of SRO30 is shown in Fig. 2. A good approximation to model the PL signal considering a small asymmetry is a Gaussian peak positioned at around 703 nm with a FWHM (full width at half maximum) of 115.8 nm (also indicted in Fig. 2).

3.2. Multilayers

All MLs were analyzed by TEM and the main finding is that only the first two layers (from the substrate side) can be easily identified. On top of these layers the layered structure is less evident due to the increased roughness caused by the SRO1 or SRO3 layers. Therefore, only Si-NCs embedded in an amorphous matrix can be observed. According to the TEM results a scheme of the structure of the multilayers can be deduced, which is shown in Fig. 3. Comparing the MLs prepared with SRO3 (M1 and M2, see Table 1) no significant and obvious differences are detected by simple inspection of the TEM micrographs (see Fig. 4 a) and b)). But performing a statistical analysis of the sizes of the Si-NCs using several micrographs a remarkable difference is observed. In the sample M1 most of the Si-NCs have sizes below 4 nm which is the thickness of the SRO3 layers, with an average size of 3.6(0.98) nm (the value in parenthesis is the estimated standard deviation) and mode size between 3.5 and 4 nm (Fig. 5a), i.e., the size of the Si-NCs is limited by the thickness of the layers. This finding is expected for thin SRO films with high Si contents as reported earlier [21]. The small size of the Si-NCs suggests that the layered structure was indeed formed despite the fact that the layered

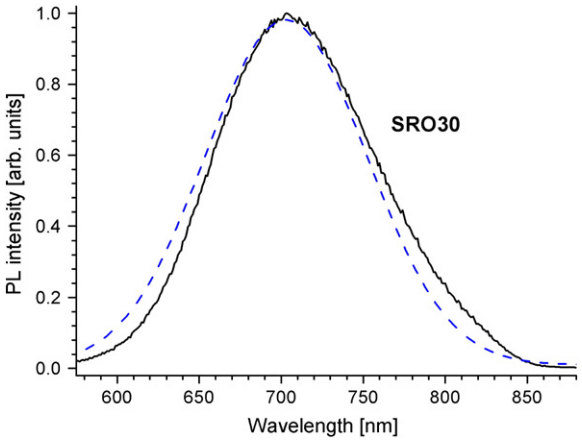

Fig. 2. PL spectrum of SRO30. The PL peak is positioned at 703 nm. The dotted line represents a Gaussian fit of the peak.

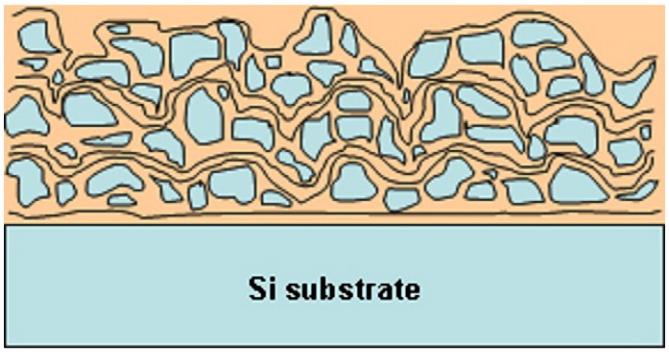

Fig. 3. Scheme of the multilayer structures. The samples can be regarded as a homogeneous distribution of Si-NCs embedded in a silicon oxide matrix.

structure could not be clearly observed in the TEM micrographs. A similar observation is made for the sample M2 where all Si-NCs exhibit sizes smaller than 8 nm which is the thickness of the SRO3 layers, and the values are typically below 5 nm (Fig. 5b) with an average size in this sample of 4.1(1.00) nm.

As for the samples M1 and M2 prepared with SRO3, in the ML synthesized with SRO1 only the first two layers can be easily identified

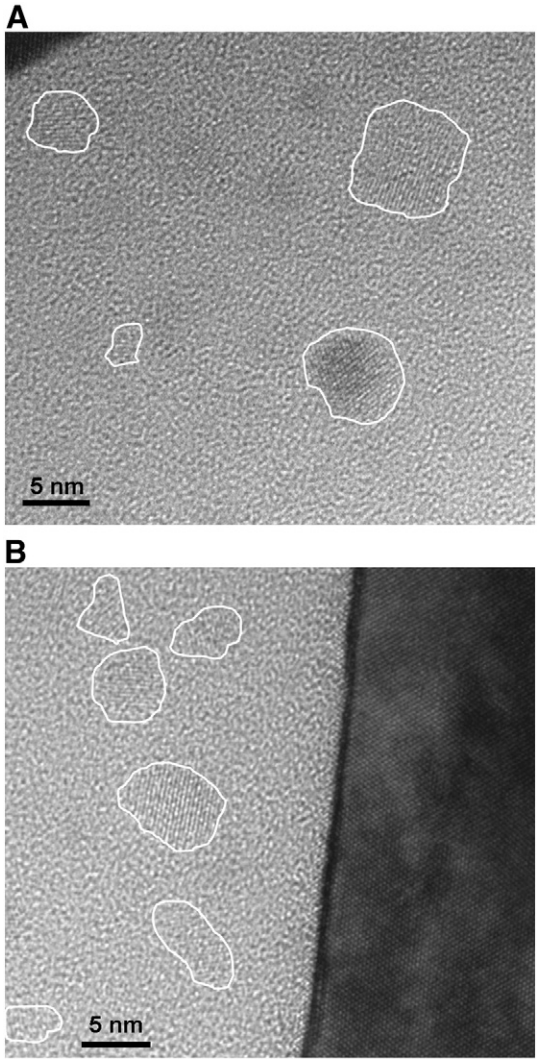

Fig. 4. Typical TEM micrographs of the samples M1 (a) and M2 (b). The black section corresponds to the Si substrate. Some layered sections can be observed in the clear part (enclosed with white lines), corresponding to the Si-NCs The average sizes of the nCs are 3.6 and 4.1 nm for samples M1 and M2 respectively.

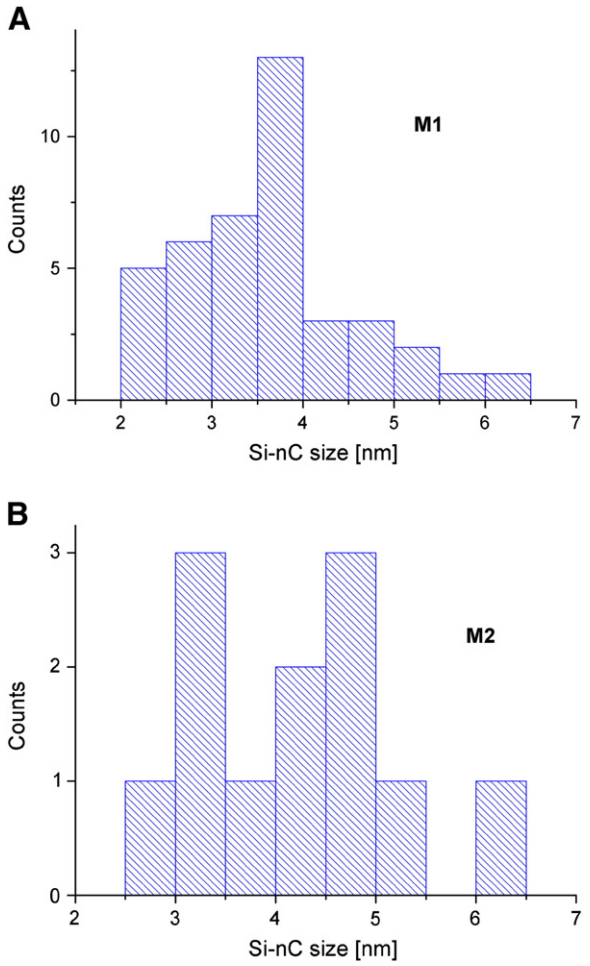

Fig. 5. Distribution of Si-nC sizes in a) M1 and b) M2. In both cases the size of the Si-NCs is typically smaller than the thickness of the SRO3 layers (4 and 8 nm respectively).

by simple inspection of the TEM micrographs (Fig. 6). But a statistical analysis (Fig. 7) clearly evidences that the mean Si-NC size is 13.4(2.97) nm, with the maximum sizes in the range of the thickness of the SRO1 layers of 22 nm. Again, the size of the Si-NCs is limited by the thickness of the layers with high Si content (SRO1).

The PL spectra of M1 and M2 are shown in Fig. 8a and b respectively. We note that the sample M3 does not show any PL signal. The PL of M1

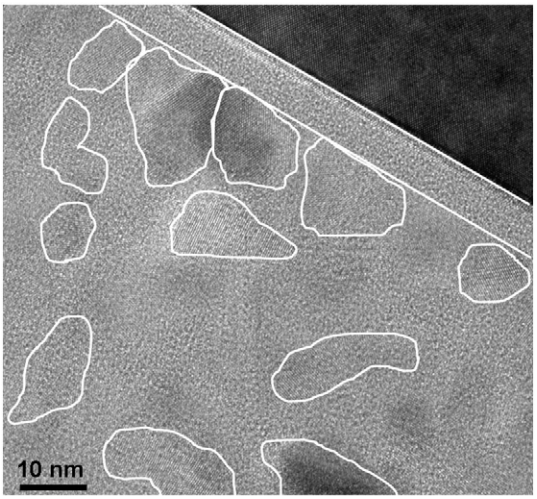

Fig. 6. Typical TEM micrograph of sample M3. The first layer of SRO50 (to the substrate's side) can be easily identified. The average size of the Si-NCs is 13.4 nm.

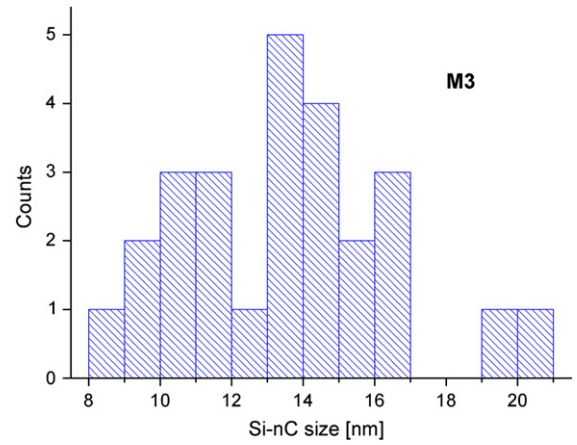

Fig. 7. Distribution of Si-NCs sizes in ML M3. All the nCs have sizes below 22 nm (the expected thickness of the SRO1 layers).

and M2 cannot originate from the layers of SRO50 because this material does not exhibit a PL emission. In addition, the PL signal cannot be due to direct band-to-band transitions, allowed by quantum confinement effects in the nanometric layers of SRO3, because the PL bands of M1 and M2 occur at the same position. As mentioned above these materials contain different Si-NC sizes and a blue-shift should occur in the PL spectrum of the sample M1 compared with that of M2 if direct

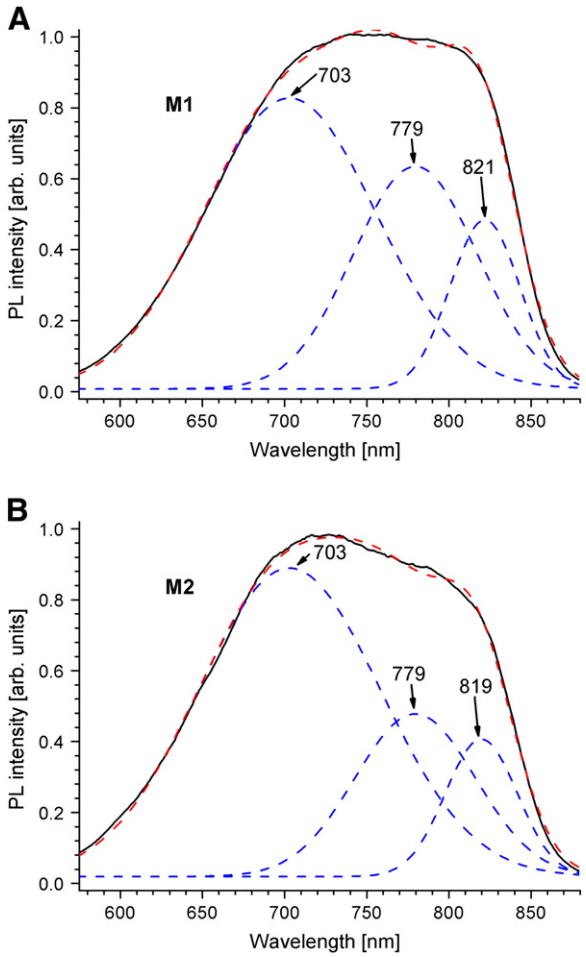

Fig. 8. Deconvoluted PL spectra of a) M1 and b) M2. Both spectra are composed of peaks positioned at around 703, 779 and 880 nm.

band-to-band transitions in the Si-NCs are responsible for the PL [12,13], which are allowed by quantum confinement effects. Other types of transitions like those involving acceptor or donor levels in the crystallites can be discarded taking into account that no doping was used during the deposition process [22]. In addition, Auger radiative recombination processes can be excluded in our system because such processes require at least two free electrons per Si-NC before excitation occurs [23]. Si-vacancies in the Si-NCs could introduce dangling bonds, but are well known as PL quenchers [24]. According to this, other transitions involving oxygen vacancies in SiO_2 tetrahedra may be responsible for the emission process. These vacancies may be regarded as "localized defects" located at the Si-SiO_x interfaces or as defects in the SiO_x matrix.

A deconvolution of the PL peaks was performed in order to give possible explanations for the occurrence of the PL signals. For both materials the PL spectra can be deconvoluted into three Gaussian peaks centred at around 703, 779 and 880 nm (bands A, B and C), as shown in Fig. 8a and b. The PL band A should have the same origin as the PL of SRO30, since this peak is also positioned at 703 nm with a FWHM similar as for SRO30 displaying a variation of up to +/−10%. Because in the sample SRO30 no Si-NCs are present, the PL signal in this material should be caused by defects in the sub-oxide matrix. We note that only an insignificant blue-shift of the PL peak was reported going from SRO Ro = 20 to Ro = 30 [6], giving evidence for the defect-related PL process. We note that this kind of defects cannot be eliminated applying standard treatments like annealing in an H_2 atmosphere. Surprisingly, the intensity of the PL signal increases after annealing in H_2 because the non-radiative defects (dangling bonds) are eliminated [25]. The large amount of sub-oxides present in SRO3 should adopt configurations similar to that in SRO30 in the transition area between SRO3 and SRO50 during the deposition of the MLs, thus allowing the occurrence of the PL band A.

The positions of the peaks B and C do not change when the size of the Si-NCs is reduced, and therefore these peaks are also not due to direct band-to-band transitions in the NCs. The areas of the PL peaks B and C increase when the size of the Si-NCs is reduced. The sum of the areas of peaks B and C amounts to 34.5% of the total area for sample M2, while the value is 43.9% for M1. The structural difference between these two samples is that the crystals in sample M1 are smaller, exhibiting a larger surface to bulk ratio and leading to a larger interface area with the silicon oxide matrix. The PL peaks B and C may originate from the interfaces between the Si-NCs and the sub-oxide matrix which is a defect-rich region [26]. Because in sample M1 the Si-NCs are smaller than in M2 the interface region is larger and consequently the PL peaks B and C are more intense for M1 than for sample M2. The sample M3 does not exhibit PL properties probably because the Si-NCs in this ML material are not small enough for this emission process. Indeed it has been reported that the PL process related to the interface region strongly depends on the NC size because quantum confinement effects in these Si-NCs are necessary [10]. Due to quantum confinement effects the band gap of the Si-NCs increases when the size decreases, and the breakdown of momentum conservation leads to pseudo-direct $\Gamma \rightarrow L$ and $\Gamma \rightarrow X$ transitions. The defect states are Γ-like and electrons excited from the Si valence band relax to the conduction band edge from which they tunnel (resonantly) to the defect states and recombine radiatively [27]. This process has been recently confirmed in a report dealing with the classification of the origin of the PL properties of Si-NCs [10]. A different model also explains the PL around 1.7 eV of Si-NCs in a silicon oxide matrix [28], but this model considers the opposite process: excitation of carriers from interfacial defects which then thermalize to the conduction band minimum of the Si-NCs to finally recombine radiatively in the valence band. Nevertheless, this model is not applicable for our system because it predicts that the energy of the PL signal varies with the size of the Si-NCs which is not observed in the MLs investigated here.

3.3. Oxidized multilayers

The sample M3 which did not present a PL signal was oxidized in dry oxygen atmosphere at different temperatures with the aim to investigate whether a reduction of the Si crystallite sizes leads to PL activity. For the annealing process the sample M3 was cut into pieces, denoted as M3a-d. The oxidation conditions applied are listed in Table 2.

Like for the non-oxidized layers, a statistical analysis of the TEM micrographs was performed for the oxidized samples to determine the Si-NC sizes. As expected, the average size of the NCs decreases with increasing oxidation temperature. This effect can be clearly seen comparing the distribution of Si-NC sizes of M3a and M3d (Fig. 9a and b respectively). An example of a TEM micrograph of M3d is displayed in Fig. 10 clearly showing that the crystals become smaller compared to the sizes shown in Fig. 6. Sample M3a contains Si-NCs with sizes up to about 20 nm with a mean size of 13.4(3.60) nm. On the other hand, for sample M3d which was heated at the highest temperature the sizes of the Si-NCs are typically smaller than 12 nm, and the estimated mean size is 10.8(3.37) nm (see Fig. 9b). According to these results it can be concluded that the oxidation level increases when increasing the oxidation temperatures, being further confirmed by ellipsometric measurements which are discussed below.

The refraction indexes of the oxidized samples calculated from the ellipsometric measurements are plotted in Fig. 11. It can be seen that the refractive index decreases with increasing oxidation temperature. Considering that the sizes of the Si-NCs and the silicon oxide zones are much smaller than the wavelength of the laser light of the ellipsometer (632.8 nm), the MLs can be regarded as an effective medium with an effective refraction index according to the Bruggeman theory [29]. The application of the Bruggeman theory is justified for the MLs because they can be viewed as a structurally homogenous distribution of Si-NCs in silicon oxide, as shown in Fig. 3. The effective refraction index of the materials (n_{eff}) is related to the refraction index of each phase (n_{Si} and n_{ox}) as well as to their volume fractions (V_{Si} and V_{ox}). The Bruggeman equation for the two-component system is:

$$V_{Si}\frac{n_{Si}-n_{eff}}{n_{Si}+2n_{eff}} = -V_{ox}\frac{n_{ox}-n_{eff}}{n_{ox}+2n_{eff}} \quad (1)$$

From this equation it is possible to obtain an approximation of the volume fraction of Si-nCs in the MLs taking into account that they are composed of Si and SiO_2, so that

$$V_{Si} + V_{ox} = 1 \quad (2)$$

Using the values $n_{ox} = 1.46$ and $n_{Si} = 3.85$, the volume fraction of Si-NCs in the different oxidized MLs is around 0.8 (M3a), 0.7 (M3b), 0.6 (M3c) and 0.2 (M3d) respectively. These results further support the observations of the TEM experiments that the oxidation level of the MLs increases when the oxidation temperature is increased, i.e., the amount of Si transformed into silicon oxides increases.

Among the oxidized samples only the samples M3c and M3d display a PL signal indicating that these materials contain Si-NCs with the adequate sizes for the PL emission. The PL emission of M3d is noisy

Table 2
Oxidation processes.

Sample	Oxidation conditions
M3a	60 min 800 °C
M3b	60 min 800 °C +30 min 900 °C
M3c	60 min 800 °C +30 min 1000 °C
M3d	60 min 800 °C +30 min 1100 °C

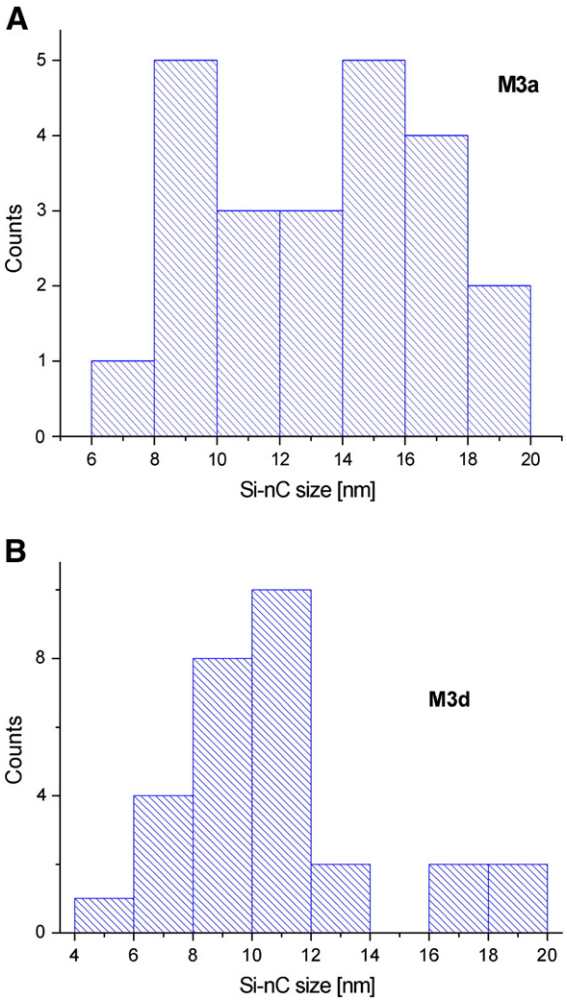

Fig. 9. Distribution of Si-NCs sizes in a) M3a and b) M3d. The nC sizes in M3d are typically smaller than 12 nm, contrary to the sizes in M3a, which range between 6 and 20 nm.

and of low intensity. Nevertheless, the spectra of the two samples can be deconvoluted into three peaks located at the same positions as in the not-oxidized materials (703, 779, and ~820 nm), as shown in Fig. 12a and b. The results suggest that the PL emission in the oxidized samples may have the same origin like in the not-oxidized samples. Upon oxidation the sub-oxides adopt a structural configuration similar

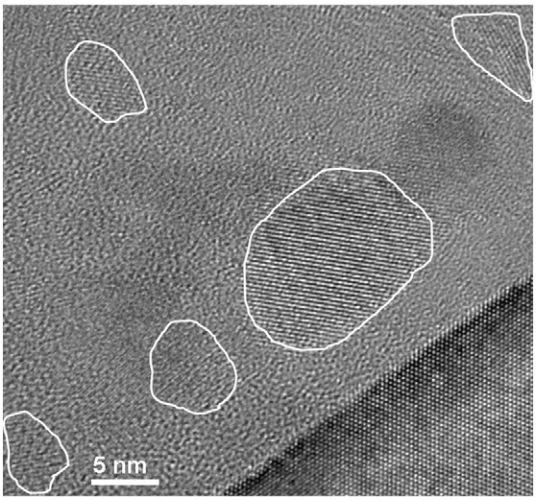

Fig. 10. Typical TEM micrograph of sample M3d.

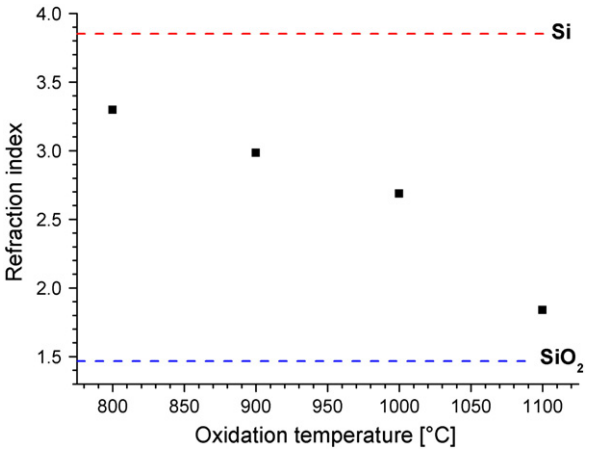

Fig. 11. Dependence of the refraction index on the oxidation temperature. The refraction index tends to that of SiO_2 when the oxidation temperature increases, indicating that the volume fraction of the Si-NCs gets smaller.

to that in SRO30, and the size of the Si-NCs is reduced also allowing the interface-related PL emission.

The sum of the areas of the peaks located at 703 and 779 nm (peaks B + C) is 48.6% of the total area for the sample M3c, while the value amounts to 32.4% for M3d. An explanation for the smaller area of the signals B and C for M3d is that a significant amount of the Si-NCs is fully oxidized reducing the intensity of the interface-related PL signal.

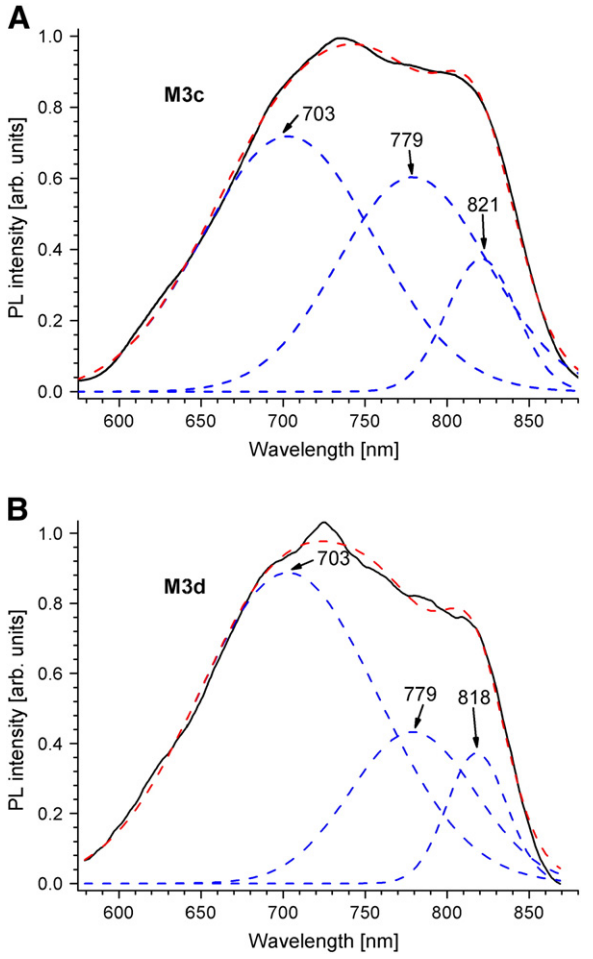

Fig. 12. PL spectra of the oxidized samples a) M3c and b) M3d. The position of the deconvoluted PL peaks is the same as in the not-oxidized samples, confirming that the origin of the PL could be the same in both cases.

4. Conclusions

ML structures containing SRO with high Si contents were prepared. We demonstrated that the size of the Si-NCs in the different structures can be tuned by varying the thickness of the layers. The Si content and size of the Si-NCs were also reduced by oxidation at elevated temperatures. The MLs containing smaller Si-NCs exhibit PL signals. All results highly indicate that the PL emission is generated by defects in the oxide matrix and by defects at the interfaces between the nanocrystals and the surrounding matrix. The first emission mechanism is independent of the existence of nanocrystals in the materials as observed for the sample SRO with Ro = 30. But the results also suggest that the interface-related PL signal depends on the size of the Si-NCs. When the Si-NCs have a size at which the band-gap of Si is pseudo-direct (a quantum confinement effect), the excited carriers can tunnel to the interfacial defects where the radiative recombination takes place.

Acknowledgements

The authors appreciate the support of CONACyT and DAAD. They also thank Pablo Alarcón from INAOE for the technical help for the oxidation of the samples.

References

[1] G. Conibeer, M. Green, R. Corkish, Y. Cho, E.C. Cho, C.W. Jiang, T. Fangsuwannarak, E. Pink, Y. Huang, T. Puzzer, T. Trupke, B. Richards, A. Shalav, K.L. Lin, Thin Solid Films 511–512 (2006) 654.
[2] G. Conibeer, M. Green, E.C. Cho, D. König, Y.H. Cho, T. Fangsuwannarak, G. Scardera, E. Pink, Y. Huang, T. Puzzer, S. Huang, D. Song, C. Flynn, S. Park, X. Hao, D. Mansfield, Thin Solid Films 516 (2008) 6748.
[3] M. Zacharias, J. Heitmann, R. Scholz, U. Kahler, M. Schmidt, J. Bläsing, Appl. Phys. Lett. 80 (2002) 661.
[4] H. Coffin, C. Bonafos, S. Schamm, N. Cherkashin, G. Ben Assayag, A. Claverie, M. Respaud, P. Dimitrakis, P. Normand, J. Appl. Phys. 99 (2006) 044302.
[5] M.L. Brongersma, A. Polman, K.S. Min, E. Boer, T. Tambo, H.A. Atwater, Appl. Phys. Lett. 72 (1998) 2577.
[6] A. Morales-Sánchez, J. Barreto, C. Domínguez-Horna, M. Aceves-Mijares, J.A. Luna-López, Sens. Act. A 142 (2008) 12.
[7] D. Riabinina, C. Durand, J. Margot, M. Chaker, G.A. Botton, F. Rosei, Phys. Rev. B 74 (2006) 075334.
[8] B. Fazio, M. Vulpio, C. Gerardi, Y. Liao, I. Crupi, S. Lombardo, S. Trusso, F. Neri, J. Electrochem. Soc. 149 (2002) G376.
[9] K.S. Min, K.V. Shcheglov, C.M. Yang, H.A. Atwater, M.L. Brongersma, A. Polman, Appl. Phys. Lett. 69 (1996) 2033.
[10] S. Godefroo, M. Hayne, M. Jivanescu, A. Stesmans, M. Zacharias, O.I. Lebedev, G. Van Tendeloo, V.V. Moshchalkov, Nat. Nanotechnol. 3 (2008) 174.
[11] Y.C. Fang, Z.J. Zhang, M. Lu, J. Lumin. 126 (2007) 145.
[12] Y. Kanzawa, T. Kageyama, S. Takeoka, M. Fujii, S. Hayashi, K. Yamamoto, Solid State Commun. 102 (1997) 533.
[13] L. Khomenkova, N. Korsunska, T. Torchynska, V. Yukhimchuk, B. Jumayev, A. Many, Y. Goldstein, E. Savir, J. Jedrzejewski, J. Phys. Condens. Matter 14 (2002) 13217.
[14] R. López-Estopier, M. Aceves-Mijares, C. Falcony, 3rd International Conference on Electrical and Electronics Engineering, IEEE, Mexico City, 2006, p. 1.
[15] E. Quiroga, W. Bensch, Z. Yu, M. Aceves, R.A. De Souza, M. Martin, V. Zaporojtchenko, F. Faupel, Phys. Stat. Sol. A 206 (2009) 263.
[16] A. Morales, J. Barreto, C. Domínguez, M. Riera, M. Aceves, J. Carrillo, Physica E 38 (2007) 54.
[17] D.J. DiMaria, J.R. Kirtley, E.J. Pakulis, D.W. Dong, T.S. Kuan, F.L. Pesavento, N. Theis, J.A. Cutro, S.D. Brorson, J. Appl. Phys. 56 (1984) 401.
[18] F.J. Himpsel, F.R. McFeely, A. Taleb-Ibrahimi, J.A. Yarmoff, G. Hollinger, Phys. Rev. B 38 (1988) 6084.
[19] F. Verpoort, P. Persoon, L. Fiermans, G. Dedoncker, L. Verdonck, J. Chem. Soc. Faraday Trans. 93 (1997) 3555.
[20] F.J. Grunthaner, P.J. Grunthaner, R.P. Vasquez, B.F. Lewis, J. Maserjian, A. Madhukar, Phys. Rev. Lett. 42 (1979) 1683.
[21] E. Quiroga, W. Bensch, M. Aceves, Z. Yu, J.P. Savy, M. Haeckel, A. Lechner, 10th International Conference on Ultimate Integration of Silicon (ULIS 2009), IEEE, Aachen, Germany, 2009, p. 349.
[22] M. Fujii, Y. Yamaguchi, Y. Takase, K. Ninomiya, S. Hayashi, Appl. Phys. Lett. 85 (2004) 1158.
[23] T. Puritis, J. Kaupuzs, Physica E 35 (2006) 16.
[24] S. Guha, M.D. Pace, D.N. Dunn, I.L. Singer, Appl. Phys. Lett. 70 (1997) 1207.
[25] R. López-Estopier, M. Aceves-Mijares, Z. Yu, C. Zuñiga, C. Falcony, 5th international conference on electrical engineering, computing science and automatic control (CCE 2008), IEEE, Mexico City, 2008, p. 489.
[26] F. Djurabekova, M. Backman, K. Nordlund, Nucl. Instrum. Meth. Phys. Res. B 266 (2008) 2683.
[27] B. Averboukh, R. Huber, K.W. Cheah, Y.R. Shen, G.G. Qin, Z.C. Ma, W.H. Zong, J. Appl. Phys. 92 (2002) 3564.
[28] S. Dhara, C.Y. Lu, K.G.M. Nair, K.H. Chen, C.P. Chen, Y.F. Huang, C. David, L.C. Chen, B. Raj, Nanotechnology 19 (2008) 395401.
[29] M. Khardani, M. Bouaïcha, B. Bessaïs, Phys. Stat. Sol. C 4 (2007) 1986.